Monte Carlo Simulation Test of Pore Blocking Effects

Aleksey Vishnyakov and Alexander V. Neimark*

The Center for Modeling and Characterization of Nanoporous Materials, TRI/Princeton, 601 Prospect Avenue, Princeton, New Jersey 08542-0625

Received November 26, 2002. In Final Form: January 21, 2003

We present a Monte Carlo (MC) simulation study of capillary condensation and desorption in a spherical cavity connected with the bulk phase by cylindrical necks of smaller diameter. We confirm two mechanisms of spontaneous evaporation from the cavity and, correspondingly, two types of adsorption hysteresis, which depend on the relation between the sizes of the cavity and the connecting pores. When the necks are sufficiently wide, evaporation from the cavity is determined by the conditions of evaporation from the neck. This is a classical ink-bottle or pore blocking effect: desorption from the cavity is controlled by the size of the neck. When the necks are narrow, evaporation from the cavity is determined by the conditions of cavitation in the stretched metastable liquid and thus does not depend on the size of blocking pores. MC simulations were performed for a Lennard-Jones fluid at the normal boiling temperature mimicking sorption of nitrogen at 77.4 K in silica mesopores. The simulation results agree with the density functional theory of capillary condensation hysteresis in spherical cavities and the experimental data reported recently (Ravikovitch, P. I.; Neimark, A. V. *Langmuir* **2002**, *18*, 1550 and 9830).

1. Introduction

The concept of pore blocking was put forward in the pioneering papers of Kraemer,[1] McBain,[2] and Cohan[3] to explain some specifics of capillary condensation hysteresis in mesoporous materials. The pore blocking implies that evaporation of the condensed liquid from a pore network is a cooperative process. Evaporation from a pore, which is connected to the bulk phase by narrower pores, is delayed and occurs spontaneously after the emptying of one of the adjacent pores. This effect of *pore blocking controlled desorption*, which is commonly called the ink-bottle effect,[4,5] is a conventional explanation of the capillary condensation hysteresis of H2 type by IUPAC classification.[5] Everett[4] and recently Rouquerol et al.[6] reviewed different aspects of pore blocking effects in great detail, mostly with examples of adsorption of vapors on porous glasses and gels.

Broekhoff and deBoer[7] developed a quantitative macroscopic description of capillary condensation hysteresis in ink-bottle pores, represented by a spherical cavity fitted with a narrow cylindrical neck. Their approach is based on Derjaguin's equations of film equilibrium.[8] They determined the pressure of spontaneous condensation in the cavity from the limit of metastability of the adsorbed film on a spherical surface. In the discussion that follows, this condensation mechanism is referred to as *near-spinodal condensation*. The pressure of evaporation was related to the formation of an equilibrium meniscus in the cylindrical neck, in accord with the conventional picture of pore blocking controlled desorption. The Derjaguin−Broekhoff−deBoer (DBdB) equations[8] describe the capillary condensation hysteresis in an ensemble of independent ink-bottle pores of different sizes. DBdB equations constitute the basis for calculating two size distributions: for the cavities from the adsorption isotherm and for the necks from the desorption isotherm. Later, Wall and Brown,[9] Mason,[10] Neimark,[11−13] and Seaton[14] developed the percolation theory of capillary condensation and desorption in pore networks. In particular, Neimark[11,12] showed that the behavior of scanning isotherms of Xe on porous glass[4] quantitatively follows the predictions of the percolation theory in a network of cavities connected by cylindrical necks.

Networking effects are not limited to the pore blocking controlled desorption. Neimark[13] suggested a mechanism of *initiated capillary condensation*. He argued that condensation in a narrow pore might result in the formation of an unstable vapor−liquid interface in the adjacent wider pore that would cause spontaneous condensation in the latter prior to the achievement of the limit of metastability of adsorption films. This effect of initiated capillary condensation may trigger an avalanche filling of the pore network.

Kadlec and Dubinin[15] and Burgess and Everett[16] related the lower closure point of adsorption hysteresis loops to the onset of cavitation in the stretched metastable liquid. *Cavitation-induced desorption* is expected to occur in

* To whom correspondence should be addressed. E-mail: aneimark@triprinceton.org.

(1) Kraemer, E. O. *Treatise on Physical Chemistry*; D. Van Nostrand: New York, 1931.
(2) McBain, J. W. *J. Am. Chem. Soc.* **1935**, *57*, 699.
(3) Cohan, L. H. *J. Am. Chem. Soc.* **1938**, *60*, 433.
(4) Everett, D. H. In *The Solid−Gas Interface*; Flood, E. A., Ed.; Marcel Dekker: New York, 1967; Vol. 2.
(5) Gregg, S. J.; Sing, K. S. W. *Adsorption, Surface Area and Porosity*; Academic Press: New York, 1982.
(6) Rouquerol, F.; Rouquerool, J.; Sing, K. S. W. *Adsorption by powders & porous solids*; Academic Press: San Diego, 1999.
(7) Broekhoff, J. C. P.; deBoer, J. H. *J. Catal.* **1968**, *10*, 153.
(8) Derjaguin, B. V. *Acta Phys.-Chim.* **1940**, *12*, 181−200.
(9) Wall, G. C.; Brown, R. J. C. *J. Colloid Interface Sci.* **1981**, *82*, 36.
(10) Mason, G. *Proc. R. Soc. London, Ser. A* **1988**, *415*, 453−486.
(11) Neimark, A. V. *Rep. Acad. Sci. USSR* (*Phys., Chem.*) **1983**, *273*, 867.
(12) Neimark, A. V. *Colloid J. USSR* **1986**, *46*, 1004.
(13) Neimark, A. V. *Stud. Surf. Sci. Catal.* **1991**, *62*, 67.
(14) Seaton, N. *Chem. Eng. Sci.* **1991**, *46*, 1865.
(15) Kadlec, O.; Dubinin, M. M. *J. Colloid Interface Sci.* **1969**, *31*, 479.
(16) Burgess, C. G. V.; Everett, D. H. *J. Colloid Interface Sci.* **1970**, *33*, 611.

10.1021/la0269107 CCC: $25.00
Published on Web 00/00/0000 PAGE EST: 7.7

mesopores blocked by micropores. The cavitation effect was not considered in the classical theories of capillary condensation hysteresis in ink-bottle pores and pore networks. A detailed analysis of cavitation-induced desorption is given recently by Ravikovitch and Neimark.[17]

During the past several years, the role of pore blocking effects in capillary condensation hysteresis has been extensively revisited using Monte Carlo (MC) and molecular dynamics (MD) simulations and density functional theory (DFT). Special attention has been paid to analyses of hysteresis in disordered materials in reference to porous glasses and silica gels,[18−22] which were considered as the case study systems for analyzing capillary hysteresis and networking effects. MC simulations of adsorption−desorption cycles in model porous glasses by Gelb and Gubbins[23] and Pellenq et al.,[19] did not display any appreciable pore blocking effects. Kierlik et al.[20,21] and Woo et al.[24] developed lattice DFT models of sorption in disordered media and constructed hysteresis loops resembling the shape of experimental adsorption isotherms on porous glasses, without invoking pore blocking effects. Qualitatively similar results were reported by Sarkisov and Monson,[22] who performed DFT calculations and MC simulations for a lattice model obtained by a coarse graining of an off-lattice model of silica gels.

Sarkisov and Monson[25] performed MD and MC simulations of capillary condensation in a single ink-bottle pore composed by a central rectangular cavity of 10σ in width connected with the bulk phase by slit micropores of 5σ in width. The hysteresis observed in this model was not related to the classical pore blocking effect. Desorption from the central cavity occurred with the connecting pores remaining filled. In this particular case, the conditions of evaporation were determined by the onset of cavitation. Maddox et al.[26] carried out MD simulations of sorption in cavities of similar rectangular shape connected by even narrower micropores which had a width of only two or three molecular diameters. The authors observed freezing in micropores that hindered adsorption in the cavity.

Ravikovitch and Neimark[27] have recently revisited the BDdB theory of capillary hysteresis in ink-bottle pores based on the nonlocal DFT[28,29] and presented experimental evidence of different pore blocking effects for adsorption of nitrogen, argon, and krypton on templated nanoporous silicas with ordered systems of cagelike pores.[17] They confirmed the DBdB scenario of capillary condensation hysteresis for ink-bottle pores with sufficiently wide necks and found that a decrease of the neck size leads to the transition from the pore blocking controlled desorption to the cavitation-induced desorption.

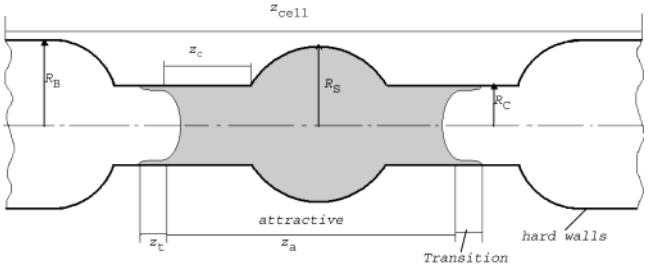

Figure 1. Ink-bottle pores used in simulations. A central spherical cavity of radius R_s is connected with the bulk phase by cylindrical necks of smaller radius R_c. The bulk reservoir is modeled as two outer hemispheres of radius R_b with hard wall repulsive walls. The attractive LJ potential is set over the distance z_c in the internal portion of the cylindrical pore. A linear decay of the attractive potential is assumed in the transition zone of length z_t. The hard wall repulsion potential is set in the outer portion of the neck and in the bulk reservoir. Periodic boundary conditions were applied in the cell.

In the present work, we perform MC simulations of capillary condensation and desorption in a spherical cavity connected with the bulk phase by cylindrical necks of a smaller diameter. We confirm two mechanisms of spontaneous evaporation from the cavity, the pore blocking controlled desorption and the cavitation-induced desorption, depending on the relation between the sizes of the cavity and the necks.

2. Simulation Details

We performed grand canonical Monte Carlo (GCMC) simulations of capillary condensation and desorption in a model ink-bottle pore. The pore geometry is shown in Figure 1. It includes a central spherical cavity of diameter H_s connected with the bulk phase by cylindrical necks of smaller diameter H_c. MC simulations were performed for a Lennard-Jones (LJ) fluid at the normal boiling temperature mimicking sorption of nitrogen at 77.4 K. The potential parameters for fluid−fluid interactions were $\sigma = 0.36154$ nm and $\epsilon/k = 101.5$ K. These parameters were found from the best fit of the equation of Johnson et al.[30] to the phase diagram for bulk nitrogen in ref 31. Although N_2 is not a spherical molecule, the LJ model reproduces quite accurately the densities of coexisting vapor and liquid, saturation pressure, and vapor−liquid surface tension of bulk nitrogen at 65 K $< T <$ 115 K.[31,32]

Following ref 33, the solid−fluid attractive potential in cylindrical pores was modeled as the integral potential from the cylindrical layer of LJ adsorption centers:[34]

$$U_{sf}^{(cyl)}(r,R) = \pi^2\rho_s\epsilon_{sf}\sigma_{sf}^2\left[\frac{63}{32}\left[\frac{R-r}{\sigma_{sf}}\left(1+\frac{r}{R}\right)\right]^{-10}F\left[-\frac{9}{2},-\frac{9}{2};1;\left(\frac{r}{R}\right)^2\right]-3\left[\frac{R-r}{\sigma_{sf}}\left(1+\frac{r}{R}\right)\right]^{-4}F\left[-\frac{3}{2},-\frac{3}{2};1;\left(\frac{r}{R}\right)^2\right]\right] \quad (1)$$

Similarly, the solid−fluid potential inside the spherical pore was modeled as the integral potential from the

(17) Ravikovitch, P. I.; Neimark, A. V. *Langmuir* **2002**, *18*, 9830−9837.
(18) Sarkisov, L.; Monson, P. A. In *Characterization of Porous Solids V*; Elsevier: Amsterdam, 2000; Vol. 128, pp 21−29.
(19) Pellenq, R. J. M.; Rodts, S.; Pasquier, V.; Delville, A.; Levitz, P. *Adsorption* **2000**, *6*, 241−249.
(20) Kierlik, E.; Monson, P. A.; Rosinberg, M. L.; Sarkisov, L.; Tarjus, G. *Phys. Rev. Lett.* **2001**, *8705*, article no.-055701.
(21) Kierlik, E.; Rosinberg, M. L.; Tarjus, G.; Viot, P. *Phys. Chem. Chem. Phys.* **2001**, *3*, 1201−1206.
(22) Sarkisov, L.; Monson, P. A. *Phys. Rev. E* **2002**, *6501*, article no.-011202.
(23) Gelb, L. D.; Gubbins, K. E.; Kaneko, K.; Kanoh, H.; Hanzawa, Y., Eds.; IK International: Chiba-City, 2002; p 333.
(24) Woo, H. J.; Sarkisov, L.; Monson, P. A. *Langmuir* **2001**, *17*, 7472−7475.
(25) Sarkisov, L.; Monson, P. A. *Langmuir* **2001**, *17*, 7600−7604.
(26) Maddox, M. W.; Quirke, N.; Gubbins, K. E. *Mol. Simul.* **1997**, *19*, 267−283.
(27) Ravikovitch, P. I.; Neimark, A. V. *Langmuir* **2002**, *18*, 1550.
(28) Tarazona, P. *Phys. Rev. A* **1985**, *31*, 2672−2679.
(29) Tarazona, P.; Marconi, U. M. B.; Evans, R. *Mol. Phys.* **1987**, *60*, 573−595.
(30) Johnson, J. K.; Zollweg, J. A.; Gubbins, K. E. *Mol. Phys.* **1993**, *78*, 591−618.
(31) Ravikovitch, P. I.; Vishnyakov, A.; Russo, R.; Neimark, A. V. *Langmuir* **2000**, *16*, 2311−2320.
(32) Ravikovitch, P. I.; Vishnyakov, A.; Neimark, A. V. *Phys. Rev. E* **2001**, *6401*, article no.-011602.
(33) Ravikovitch, P. I.; ODomhnaill, S. C.; Neimark, A. V.; Schuth, F.; Unger, K. K. *Langmuir* **1995**, *11*, 4765−4772.
(34) Tjatjopoulos, G. J.; Feke, D. L.; Mann, J. A. *J. Phys. Chem.* **1988**, *92*, 4006−4007.

Table 1. Dimensions of the Ink-Bottle Pores

parameter		parameter value, [σ] pore I	pore II	pore III
$H_s = 2R_s$	sphere diameter	15.8	15.8	15.8
$H_c = 2R_c$	cylinder diameter	11.0	11.0	9.0
z_c	"attractive" cylinder length	10.1	20.1	10.1
z_{cell}	total cell length	60.0	80.0	60.0
z_a	length of attractive zone	36.0	56.0	36.0
z_t	length of transition zone	4.0	4.0	4.0
$H_b = 2R_b$	"bulk" sphere diameter	25.0	25.0	25.0

spherical layer of LJ adsorption centers:[27]

$$U_{sf}^{(sph)}(r,R) = 2\pi\rho_s\epsilon_{sf}\sigma_{sf}^2\left[\frac{2}{5}\sum_{i=0}^{9}\left(\frac{\sigma_{sf}^{10}}{R^i r^{10-i}} + (-1)^i\frac{\sigma_{sf}^{10}}{R^i(r-2R)^{10-i}}\right) - \sum_{i=0}^{9}\left(\frac{\sigma_{sf}^{4}}{R^i r^{4-i}} + (-1)^i\frac{\sigma_{sf}^{4}}{R^i(r-2R)^{4-i}}\right)\right] \quad (2)$$

In eqs 1 and 2, r is the radial coordinate of the fluid molecule reckoned from the pore center, $R = H/2$ is the radius of the cylindrical (eq 1) or spherical (eq 2) pores, ρ_s is the surface number density of the adsorption centers, ϵ_{sf} and σ_{sf} are the effective LJ parameters of solid−fluid interactions, and $F[\alpha,\beta,\gamma,\delta]$ is the hypergeometric function. As the pore width increases, the potentials (1,2) reduce to the 10−4 form of the potential with a plane of LJ centers. The LJ parameters of the potential $\sigma_{sf} = 0.3494$ nm and $\epsilon_{sf}/k = 53.22$ K and $\rho_s = 15.3$ nm^{-2} were found in ref 33 from the best fit of the calculated nitrogen adsorption isotherm on the flat surface to the experimental isotherm on nonporous silica.[35]

To provide for a continuous solid−fluid potential at the pore intersection, the isopotential surfaces in the spherical pore were connected with the isopotential surfaces on the cylindrical pore at the same potential level. In the vicinity of the intersection of the isopotential surfaces for the spherical and cylindrical pores, the isopotential surfaces were smoothed by gyration paraboloids.

The bulk reservoir was modeled as two outer hemispheres of diameter H_b with hard wall repulsive walls. To provide for a smooth transition from the wetting pore walls to the bulk reservoir, we use a piecewise solid−fluid potential in the connecting cylinder. The attractive LJ potential (2) was set over the distance z_c in the internal portion of the neck. The hard wall repulsion potential was set in the outer portion of the neck. The linear decay of the attractive potential was assumed in the transition zone of length z_t. The total length of the simulation cell was $z_{cell} = (H_s^2 - H_c^2)^{1/2} + l_c + (H_b^2 - H_c^2)^{1/2}$. The length of the central attractive pore was $z_{attr} = (H_s^2 - H_c^2)^{1/2} + z_c$. Periodic boundary conditions were applied in the cell.

GCMC simulations were performed according to the standard scheme.[36] We constructed adsorption and desorption isotherms in three cells of ink-bottle geometry. The geometrical parameters of the cells are given in Table 1 in molecular diameters of fluid. The size of the cavity was 15.8σ. The neck dimensions varied. Pore I had wide-and-short necks of 11σ in width and of 10.1σ in "attractive" length. In pore II with wide-and-long necks, the attractive length was extended to 20.1σ. In pore III with narrow-and-short necks, the neck diameter was reduced to 9σ and the attractive length of 10.1σ was the same as in pore I.

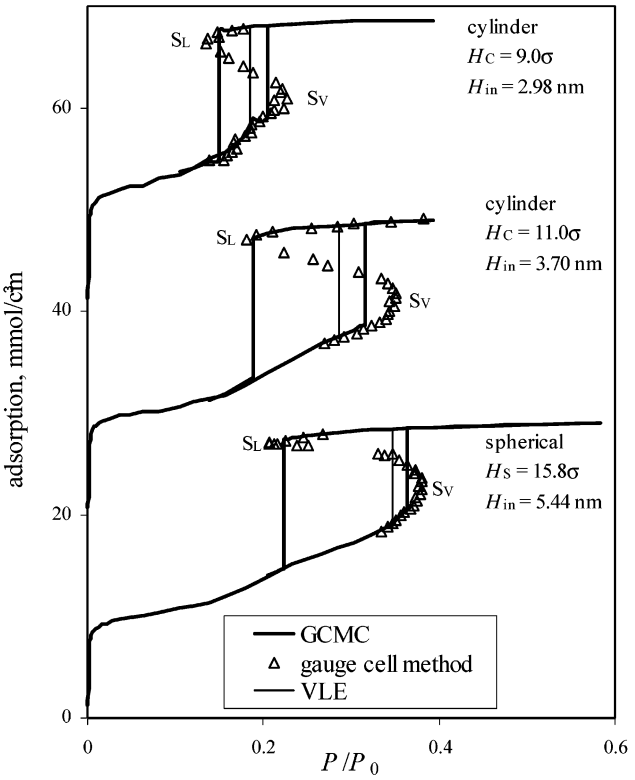

Figure 2. The adsorption isotherms in the individual pores that form the ink-bottle pores I, II, and III depicted in Figure 1. Thick solid lines show the GCMC isotherms that form a hysteresis loop. The vertical steps correspond to the spontaneous capillary condensation and desorption transitions observed in GCMC simulations. Symbols show the results obtained with the gauge cell MC simulation method. Thin vertical lines correspond to the locations of vapor−liquid equilibria determined from the Maxwell rule. $H_{in} = H_c - \sigma_{sf}$ denotes the "internal" diameter of a spherical or cylindrical pore; S_V and S_L indicate the vaporlike and liquidlike spinodals.

Depending on the chemical potential, the number of fluid particles in the ink-bottle pores varied from almost zero up to ca. 3500. Special care was taken during the simulation of the desorption process, which is associated with formation and movement of equilibrium vapor−liquid interfaces. In the vicinity of these stepwise transitions, the equilibration is fairly slow. Therefore, we had to adjust the simulation length for each particular pore and conditions. The equilibration was performed using a series of consecutive stages each of which included 10 million GCMC steps (one step consisted of a trial particle displacement, insertion, and removal). To trace the desorption, moving average density over 1 million GCMC steps was calculated. If no decrease in the number of molecules was observed within 10 million steps, the averaging over 5×10^4 GCMC steps per molecule was started. Otherwise, the equilibration continued for another stage of 10 million GCMC steps.

We constructed reference isotherms for the individual pores (the spherical cavity of 15.8σ in diameter and two cylindrical pores of 9σ and 11σ in diameter) that form the ink-bottle pores described above. Stable and metastable parts of adsorption isotherms were generated by GCMC. A typical GCMC run involved about 8×10^4 steps per fluid molecule (each step consisted of a trial molecule displacement, insertion, and removal); the averaging was performed over the last 5×10^4 steps per molecule. The

(35) deBoer, J. H.; Linsen, B. G.; Osinga, T. J. *J. Catal.* **1965**, *4*, 643.
(36) Allen, M. P.; Tildesley, D. J. *Computer simulation of liquids*; Clarendon Press: Oxford, 1987.

Table 2. Conditions of VLE, GCMC Spontaneous Condensation and Evaporation, and Vaporlike and Liquidlike Spinodals in the Individual Spherical and Cylindrical Pores

pore shape, diameter	liquid spinodal P_{SL}/P_0	spontaneous desorption/ cavitation P_{cav}/P_0	equilibrium (VLE) P_e/P_0	spontaneous condensation P_{cond}/P_0	vapor spinodal P_{SV}/P_0
spherical, $H = 16\sigma$	0.206	0.220	0.347	0.369	0.385
cylindrical, $H = 11\sigma$	0.181	0.188	0.285	0.319	0.351
cylindrical, $H = 9\sigma$	0.134	0.149	0.183	0.204	0.236

last configuration of the GCMC run at a given chemical potential served as the starting configuration for the simulation of the next point on the adsorption isotherm. In all three pores, the GCMC isotherms consisted of adsorption and desorption branches that formed prominent hysteresis loops. To obtain the conditions of vapor−liquid equilibrium (VLE), we connected the adsorption and desorption branches of GCMC isotherms by continuous trajectories of equilibrium metastable and unstable states using the gauge cell MC method.[37,38] The gauge cell MC method implies a thermal and chemical equilibrium between the pore cell and a gauge cell of limited capacity. The limited capacity of the gauge cell constrains the density fluctuations in the pore and allows one to keep the fluid in the pore in a state that would be unstable in an open system. The chemical potential in the pore fluid is determined from the equation of state of the fluid in the gauge. We used the bulk LJ gas as a reference (gauge) system and the equation of Johnson et al.[30] as the equation of state. The size of the gauge cell was adjusted for each simulation so that the gauge cell contained ca. 40 fluid molecules. Each simulation run included an equilibration stage of ca. 4×10^4 steps per molecule and an averaging stage of the same length. Each step included attempts of molecule displacement in each cell and two attempts of a molecule transfer between the cells. To obtain the next point on the isotherm, the last configuration of the previous run served as the starting configuration and several molecules were added to the gauge.

3. Results and Discussion

3.1. Sorption in Single Spherical and Cylindrical Pores. In Figure 2, we presented the MC isotherms in the spherical cavity of 15.8σ in diameter and two cylindrical pores of 9σ and 11σ in diameter. Solid curves represent the GCMC adsorption and desorption isotherms. Vertical steps correspond to the pressures of spontaneous condensation, P_{cond}, and desorption, P_{cav}. Since the periodic boundary conditions were applied, desorption from the cylindrical pores occurred spontaneously at the onset of cavitation in a like manner as desorption from the cavity. The van der Waals type, sigmoid isotherms generated by the gauge cell MC method are depicted by open triangles. The gauge cell MC method extends the GCMC metastable states up to their true limits of stability. The turnover point of the adsorption isotherm determines the vaporlike spinodal, S_V. The turnover point of the desorption isotherm determines the liquidlike spinodal, S_L. The backward trajectory connecting the spinodals corresponds to a sequence of unstable states, which cannot be realized in an open system during GCMC simulations. The condition of equilibrium between vaporlike states (adsorption films) and liquidlike states (condensed phase) is given by the Maxwell rule of equal areas. The pressure P_e of VLE is shown by a thin vertical line. The values of characteristic pressures are given in Table 2.

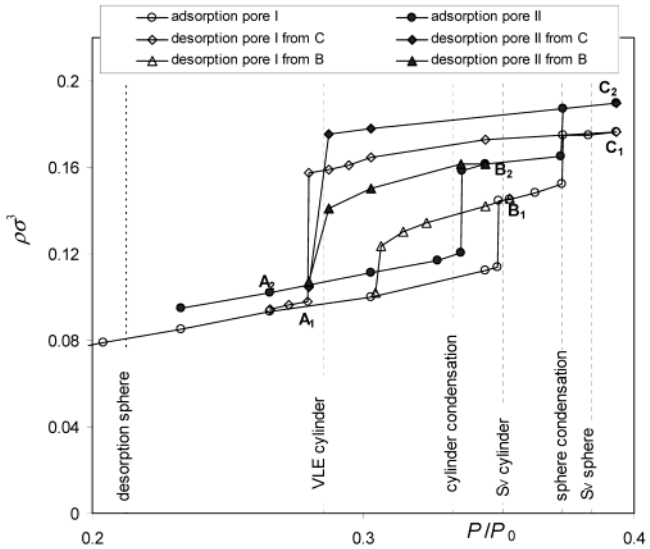

Figure 3. Adsorption−desorption isotherms for pores I and II. Dotted vertical lines show the characteristic pressures for the reference 15.8σ spherical cavity and 11σ cylindrical channel. Outer desorption isotherms originate from points C_1 and C_2 of complete filling. Scanning desorption isotherms originate from states B_1 and B_2, which correspond to liquidlike plugs condensed in the necks and a vaporlike filling of the cavity. Evaporation from the filled ink-bottle pore occurs in one step close to the VLE pressure for the reference cylindrical pore, thusu exhibiting a classical pore blocking effect.

The values of P_{cav} and P_{cond}, determined in GCMC simulations, are not clearly defined thermodynamic parameters. They are determined by the conditions of nucleation and may depend on the simulation protocol, particularly on the length of the simulation run. However, beyond the very vicinity of the hysteresis critical temperature, the hysteresis loops observed in GCMC simulations are reproducible, and deviations of P_{cav} and P_{cond} in different simulation runs are negligible.[38,39]

3.2. Sorption in Ink-Bottle Pores. What may we expect? On the basis of the discussion given in the Introduction, we may expect that the capillary condensation in ink-bottle pores should proceed in two stages. Condensation in the necks should occur first. Since the neck represents a finite length cylinder, the condensation in the neck happens spontaneously at a pressure, P_{cond}^{neck}, intermediate between the pressures of the vaporlike spinodal and spontaneous condensation determined for the reference cylinder with periodic boundary conditions, $P_{cond}^{cyl} < P_{cond}^{neck} < P_{SV}^{cyl}$. The shorter the pore, the closer P_{cond}^{neck} to P_{SV}^{cyl}.

Condensation in the cavity should occur near the pressure of spontaneous condensation in the reference spherical pore, $P_{cav}^{cav} \approx P_{cav}^{sph}$. The mechanism of desorption depends on the size of the necks. Desorption from an open-ended cylindrical pore occurs at the conditions of formation of an equilibrium meniscus, that is, at $P_{des}^{neck} \approx P_e^{cyl}$. Thus,

(37) Neimark, A. V.; Vishnyakov, A. *Phys. Rev. E* **2000**, *62*, 4611−4622.

(38) Vishnyakov, A.; Neimark, A. V. *J. Phys. Chem. B* **2001**, *105*, 7009−7020.

(39) Neimark, A. V.; Ravikovitch, P. I.; Vishnyakov, A. *J. Phys.: Condens. Matter* **2003**, *15*, 347−365.

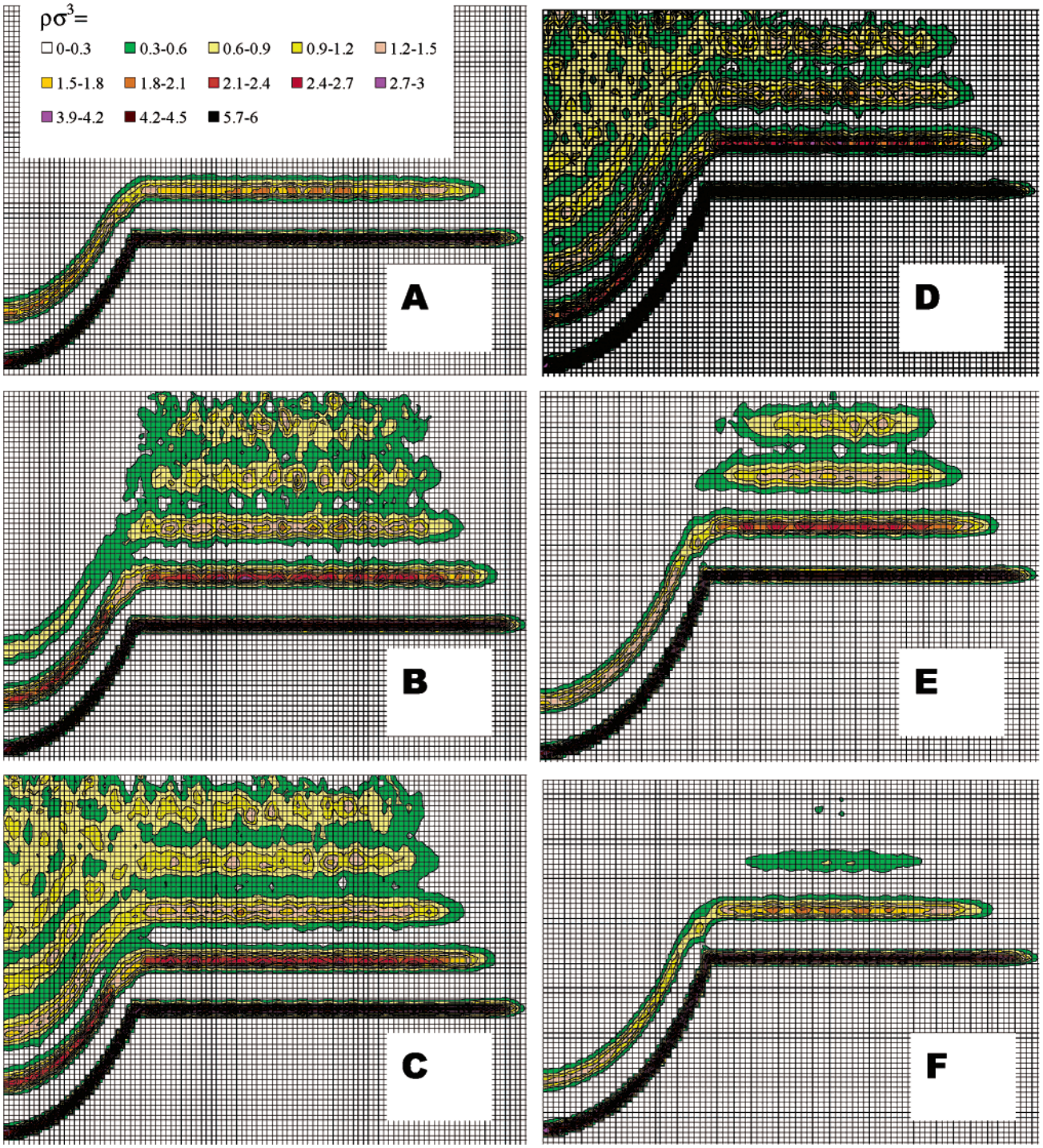

Figure 4. Local density profiles. On each profile, the center of the spherical pore corresponds to the left upper corner. The upper edge corresponds to axis *z*, which is the pore symmetry axis (see also Figure 1). Left panels (A, B, C): adsorption in pore I. (A) Point A_1 in Figure 3 (an adsorbed film in the spherical cavity and the cylindrical neck). (B) Point B_1 in Figure 3 (after the condensation in the neck: a liquidlike plug condensed in the neck in equilibrium with a film in the cavity). (C) Point C_1 in Figure 3 (after the condensation in the cavity: a liquidlike state in the pore, complete filling). Right panels (E, D, F): desorption in pore III. (D) Point D in Figure 6 (a liquidlike state in the pore, complete filling). (E) Point E in Figure 6 (after the cavitation-induced evaporation from the cavity: a liquidlike plug remains in the neck in equilibrium with a film in the cavity). (F) Point F in Figure 6 (after the evaporation of the plug: an adsorbed film in the spherical cavity and the cylindrical neck).

in the case of pore blocking controlled desorption, evaporation from an ink-bottle pore should happen in one step at P_e^{cyl}. The condition of this regime is $P_{cav}^{sph} < P_e^{cyl} < P_e^{sph}$. This inequality is valid for the cylindrical pore of $H = 11\sigma$, so that we may expect to observe the pore blocking controlled desorption in ink-bottle pores I and II.

In the case of necks so narrow that $P_e^{cyl} < P_{cav}^{sph}$, evaporation from the cavity should happen at the onset of cavitation, near P_{cav}^{sph}. When the cavity is emptied, liquid plugs may remain in the necks. The plug shaped as a thin liquid bridge evaporates at a pressure $P_{des}^{neck} > P_e^{cyl}$ exhibiting the second step on the desorption isotherm. The shorter the pore, the closer P_{des}^{neck} to P_{cav}^{sph}.

Inequality $P_e^{cyl} < P_{cav}^{sph} < P_{SV}^{cyl}$ fulfills for the cylindrical pore of $H = 9\sigma$. Thus, in the ink-bottle pore III, we may

expect to observe the cavitation-induced regime of desorption. The hysteresis loop should have two steps on both branches.

A special case is distinguished for the necks so narrow that $P_{SV}^{cyl} < P_{cav}^{sph}$, that is, the pressure of evaporation from the cavity exceeds the pressure of condensation in the necks. In this situation, the condensation−desorption cycle should produce the isotherm with two separated hysteresis loops. If the diameter of the cylindrical neck is smaller than the pore hysteresis critical size, condensation in the neck proceeds without hysteresis.[40] In this case, the isotherm in the ink-bottle pore should contain a reversible step corresponding to the condensation in the necks and a hysteresis loop corresponding to the condensation in the cavity. This type of isotherm was generated in ref 25 for a model ink-bottle pore of a rectangular shape. A reversible isotherm with two consecutive steps is expected if the cavity size is smaller than the hysteresis critical size. In all these situations, sorption in the cavity is not affected by the necks.

3.3. Sorption in Ink-Bottle Pores: Results of Simulations. GCMC simulations performed for the ink-bottle pores I, II, and III confirm the above predictions in full.

Condensation in Pores I and II. In Figure 3, we present the GCMC isotherms for pores I and II. As the pressure increases, an adsorbed film grows on the pore walls. At $P = 0.303P_0$, we observe a typical vaporlike state with a film coating pore walls. The density profile of this state for pore I is given in Figure 4a. At $P_0 = P_{cav}^{neck} = 0.350P_0$, the fluid in pore I condenses in the attractive part of the neck, while the film in the cavity is still stable (Figure 4b). The concave menisci at the connection between the cavity and the neck and in the neck's transition zone are easily seen in Figure 4b. As expected, the condensation in the neck occurred very close to the vaporlike spinodal for the 11σ cylindrical pore, $P_{cond}^{neck} \approx P_{SV}^{cyl}$.

As the pressure increases further, the adsorbed film in the cavity continues to build up. The menisci in the necks advance a little and flatten. At $P_{cav}^{cav} = 0.373P_0$, the fluid condenses in the cavity into a liquidlike state. The density profile for this state is shown in Figure 4c. As expected, the condensation occurred very close to the point of spontaneous condensation in the reference spherical pore, $P_{cav}^{cav} \approx P_{cav}^{sph}$ (Table 2).

The influence of the neck width on the sorption hysteresis in ink-bottle pores was checked on pore II. In pore II, the neck's attractive zone was twice as long as in pore I (see Figure 1 and Table 1). The adsorption isotherm is qualitatively similar to that in pore I. As expected, the condensation in the longer neck occurred near the point of spontaneous condensation in the reference cylindrical pore, $P_{cond}^{neck} \approx P_{cond}^{cyl}$ (see Figure 2, Table 2). For both pores I and II, inequality $P_{cond}^{cyl} < P_{cond}^{neck} < P_{SV}^{cyl}$ fulfills. Condensation in the cavity occurred at the same pressure as in pore I.

Desorption in Pores I and II. For pore I, we constructed two desorption isotherms. The outer desorption isotherm started from point C of complete filling of the whole pore by a liquidlike state (see Figure 3). The scanning desorption isotherm started from point B of incomplete filling, which corresponds to a liquidlike plug condensed in the necks in equilibrium with a three-layer adsorbed film in the cavity (Figure 4b).

On the outer desorption branches in both pores I and II, the fluid evaporated in one step at $P/P_0 \approx 0.280$, which is close to the pressure of vapor−liquid coexistence for the reference cylindrical pore, $P_{des}^{neck} \approx P_e^{cyl} = 0.285P_0$ The neck and the cavity were emptied almost at once. The desorption started from the formation of an equilibrium meniscus and its receding from the transition zone between the attractive and repulsive parts of the necks to the cavity, similar to earlier observations of Marconi and van Swol.[41] When the meniscus reached the neck−cavity intersection, the fluid in the cavity, which was far beyond the vapor−liquid equilibrium for the reference spherical pore, evaporated spontaneously. This is a prominent example of pore blocking controlled desorption: Evaporation from a pore, which is connected to the bulk phase by narrower pores, is delayed and, thus, occurs spontaneously after the emptying of one of the adjacent pores. A sequence of snapshots presented in Figure 5 shows the dynamics of the pore blocking controlled desorption observed in pore I.

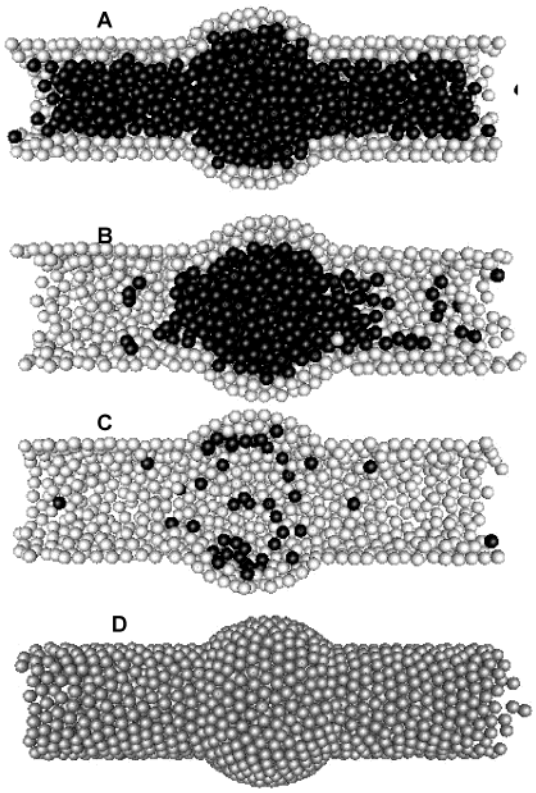

Figure 5. Pore blocking controlled desorption. Snapshots of the receding meniscus in the process of desorption in pore I (point E to point F) at $P = 0.280P_0$. Pore walls are not shown. (A) Initial configuration of complete filling in the beginning of the simulation run. This configuration represents the final equilibrium configuration generated at $P = 0.287P_0$. The fluid is condensed in the cavity and in the attractive part of the neck. The meniscus is located in the transition zone of the neck. (B) after 10^7 GCMC steps. The meniscus has receded to the neck−cavity joint; the cavity is still completely filled. (C) After 6×10^7 GCMC steps. The fluid has evaporated from the cavity; an equilibrium adsorption film is left behind. (D) The same as panel C from the outside. A hexagonal order in the contact layer of the adsorbed film is well pronounced. On panels A, B, and C, the "inner" atoms (which are removed from the pore in the course of the desorption transition) are shown in black. The "outer" atoms (which belong to the film on the pore walls that remains after the transition) are shown in light gray.

(40) Neimark, A. V.; Ravikovitch, P. I.; Vishnyakov, A. *Phys. Rev. E* **2000**, *62*, R1493−R1496.

(41) Marconi, U. M. B.; van Swol, F. *Europhys. Lett.* **1989**, *8*, 531−535.

(42) Kozak, E.; Chmiel, G.; Patrykiejew, A.; Sokolowski, S. *Phys. Lett. A* **1994**, *189*, 94−98.

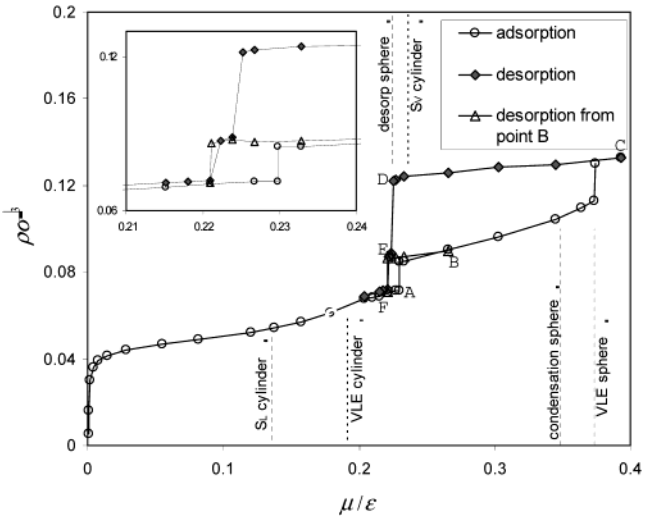

Figure 6. Adsorption−desorption isotherms for ink-bottle pore III. Dotted vertical lines show the characteristic pressures for reference 15.8σ spherical pore and 9σ cylindrical channel. The outer desorption isotherm originates from state C of complete filling. The scanning desorption isotherm originates from state B, which corresponds to a liquidlike plug condensed in the necks and a vaporlike filling of the cavity. Evaporation from the filled ink-bottle pore occurs in two steps. The first step (point D to point E) corresponds to the cavitation-induced evaporation from the cavity with liquidlike plugs remaining in the necks, and the second step (point E to point F) corresponds to the evaporation of the plugs in the necks.

On the scanning desorption isotherm in pore I, a stepwise evaporation of the plug in the pore neck occurred at $P \approx 0.306P_0$. This pressure is substantially higher than the pressure of vapor−liquid coexistence in the reference cylindrical pore $P_e^{cyl} = 0.285$ (Figure 3). We see that evaporation of the liquidlike condensate from a cylindrical channel with two ends open to the vapor phase proceeds differently than from a channel with one open end and the other connected to the filled cavity. The neck in pore I was too short to accommodate a liquidlike plug with two equilibrium menisci, and thus, evaporation occurred spontaneously prior to the formation of equilibrium menisci. This explanation is confirmed by simulations in pore II, which has a longer neck.

We generated a scanning desorption isotherm in pore II similarly to the scanning isotherm in pore I (Figure 3). In this case, however, evaporation of the plug occurred at $P \approx 0.284 \pm 0.003\ P_0$, close to the pressure of the vapor−liquid equilibrium P_e^{cyl} for the reference infinite cylinder. That is, the neck length was sufficient for the formation of equilibrium menisci on both of the plug edges. We conclude that while the length of the neck does not appreciably affect the evaporation from the filled cavity, the evaporation from the neck with the unfilled cavity does depend on the neck length. The longer the channel, the closer the desorption pressure to the VLE pressure in the infinite cylinder.

Condensation in pore III proceeds in two steps, in the same fashion as in pores I and II (Figure 6). The first condensation step at $P = 0.228P_0$ corresponds to the formation of a liquidlike plug in the neck. As expected, similar to pore I, the condensation in the neck occurred very close to the vaporlike spinodal for the 9σ cylindrical pore, $P_{cond}^{neck} \approx P_{SV}^{cyl}$. The second step corresponds to the condensation in the cavity, which occurred at $P = 0.373P_0$, close to the pressure of spontaneous condensation in the reference individual cavity, $P \approx P_{cond}^{sph}$.

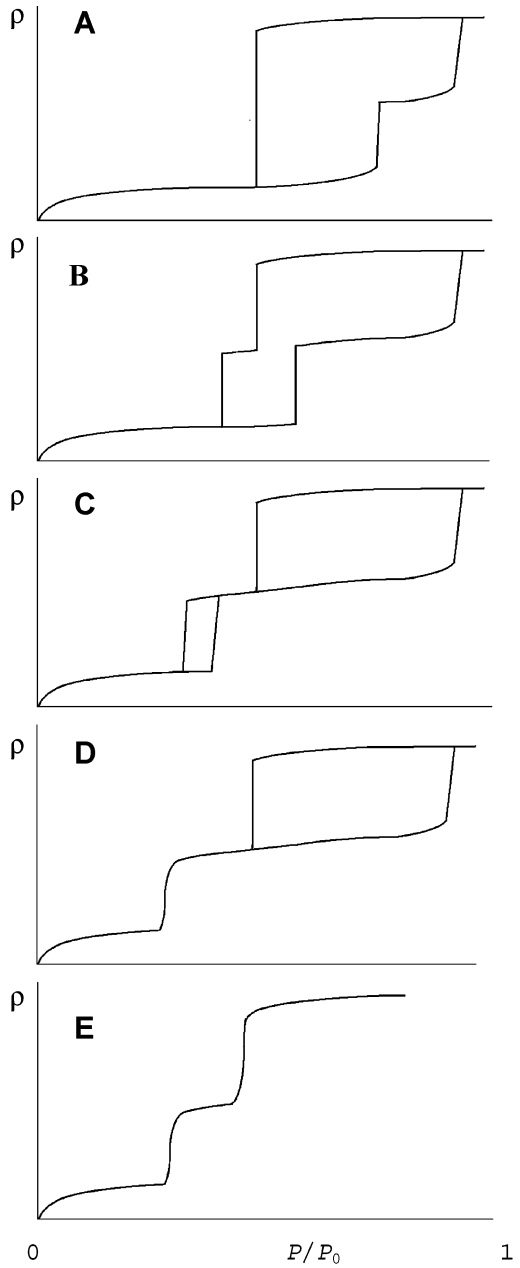

Figure 7. Schematic types of adsorption isotherms in a pore where a wider pore is connected with an equilibrium bulk by a narrow pore. (A) Pore blocking controlled desorption, $P_{des}^{(n)} < P_{des}^{(w)} < P_e^{(n)} < P_e^{(w)}$; desorption in both pores occurs simultaneously at $P_e^{(n)}$. (B) $P_{des}^{(n)} < P_e^{(n)} < P_{des}^{(w)}$, desorption from the wider pore at $P_{des}^{(w)}$ precedes the desorption from the narrower pore at $P_e^{(n)}$. (C) $P_e^{(n)} < P_{cond}^{(n)} < P_{des}^{(w)} < P_{cond}^{(w)}$; the isotherm has two separate hysteresis cycles for wider and narrower pores. (D) The same as (C), but $P_e^{(n)} = P_{cond}^{(n)}$; the hysteresis for the narrower pore disappears (e.g., in narrow pores or in pores with close ends (refs 25, 41, and 42)). (E) The same as (D), but $P_e^{(w)} = P_{cond}^{(w)}$; hysteresis for the wider pore also disappears.

Desorption in Pore III. In Figure 6, we present the outer and scanning desorption isotherms. The scanning desorption isotherm, started from point B of incomplete filling, was qualitatively like the scanning isotherm in pore I. Evaporation of the liquidlike plug in the neck occurred at $P = 0.220P_0$, above the pressure of the vapor−liquid equilibrium P_e^{cyl} for the reference infinite cylinder, as expected for short necks.

The desorption isotherm, started from point C of complete filling, exhibits two stepwise desorption transi-

tions (Figure 6). In the first stage, the spontaneous cavitation in the cavity occurs at $P = 0.225P_0$ (from point D), very close to the pressure of cavitation in the reference spherical pore, $P_{cav}^{cav} \approx P_{cav}^{sph}$ (see Table 2). After the emptying of the central part of the cavity, a two-layer adsorbed film remains. At the same time, a liquidlike plug in the neck is still present, as demonstrated in Figure 4e. This state falls exactly onto the scanning desorption isotherm, thus confirming that we deal with an equilibrium state. The second desorption transition (point E to point F) that corresponds to the evaporation of the plug occurred at $P = 0.220P_0$, at the same point as on the scanning isotherm. After the emptying of the central part of the neck, a two-layer adsorbed film remains on the pore walls (Figure 4f). Pore III represents a prominent example of the cavitation-driven desorption: evaporation from the cavity precedes evaporation from the necks. Capillary condensation hysteresis in the cavity is practically identical to that in the reference spherical pore and does not depend on the dimensions of the neck.

4. Conclusions

We performed Monte Carlo simulations of capillary condensation and desorption to confirm different mechanisms of sorption hysteresis in ink-bottle pores. An ink-bottle pore was modeled as a spherical cavity connected with the bulk phase by cylindrical necks of smaller diameter. Simulations were done for a LJ fluid interacting with wetting pore walls through the integrated potential from either the spherical (in cavities) or the cylindrical (in necks) layer of attractive LJ centers distributed with an average density. The parameters of fluid−fluid and fluid−solid interactions were chosen to mimic sorption of nitrogen at the normal boiling temperature of 77.4 K in silica pores. Three ink-bottle pores with the cavity of 15.8σ in diameter and different necks were studied. Pore I had wide-and-short necks of 11σ in width and of 10.1σ in length. In pore II with wide-and-long necks, the neck length was extended to 20.1σ. In pore III with narrow-and-short necks, the neck diameter was reduced to 9σ. Reference sorption isotherms were generated in the single spherical cavity of 15.8σ in diameter and the cylindrical channels of 9σ and 11σ in diameter with periodic boundary conditions.

Two mechanisms of spontaneous evaporation from the cavity and, correspondingly, two types of adsorption hysteresis were observed depending on the relation between the sizes of the cavity and the connecting pores. The *pore blocking controlled* regime of desorption was observed in pores I and II with sufficiently wide necks. Evaporation from the pore occurred in one step, at the conditions of formation of an equilibrium receding meniscus in the pore neck. The corresponding type of adsorption isotherm is schematically depicted in Figure 7A. The *cavitation-induced* regime of desorption was observed in pore III with narrower necks. Evaporation from the cavity occurred at the onset of cavitation of the stretched metastable liquid, prior to the emptying of the necks. Desorption from the necks resulted in the second step on the desorption isotherm (Figure 7B).

Comparing the pressures of evaporation transitions in the ink-bottle pores and in the reference spherical and cylindrical pores, we formulated the conditions of these hysteresis regimes. The *pore blocking controlled* regime of desorption is expected to happen when the pressure of the equilibrium meniscus formation in the cylindrical neck exceeds the pressure of cavitation in the spherical pore, $P_{cav}^{sph} < P_e^{cyl}$. The *cavitation-induced* regime of desorption is expected to happen when the necks are so narrow that the opposite inequality, $P_e^{cyl} < P_{cav}^{sph}$, holds true and, thus, the evaporation from the cavity does not depend on the size of blocking pores. We have also formulated the conditions of other hysteresis regimes, which may be observed in ink-bottle pores of special geometries. The conclusions from present MC simulations agree with the nonlocal density functional theory (NLDFT) of capillary condensation hysteresis in spherical cavities and with experimental data.[17,27]

As an auxiliary result, we have established interesting features of capillary condensation and evaporation of liquidlike plugs in finite length open-ended cylindrical pores. In sufficiently long necks, the condensation occurs close to the conditions of spontaneous condensation in reference cylindrical channels with periodic boundary conditions applied, $P_{cond}^{neck} \approx P_{cond}^{cyl}$. As the pore length decreases, the condensation takes place closer to the conditions of the vaporlike spinodal in the reference pore, $P_{cond}^{neck} \approx P_{SV}^{cyl}$. While desorption from a cylindrical pore with one open end is expected to occur at the condition of formation of the equilibrium meniscus, evaporation of liquidlike plugs depends on the plug length. The shorter the neck, the closer the evaporation pressure to the pressure of condensation. In general, the following inequalities fulfill: $P_{cond}^{cyl} < P_{cond}^{neck} < P_{SV}^{cyl}$ and $P_e^{cyl} < P_{des}^{neck} < P_{cond}^{neck}$.

Acknowledgment. We thank P. I. Ravikovitch for multifarious discussions. The work was supported by the TRI/Princeton exploratory research program.

LA0269107